Original scientific paper

COMPARISON OF NONCLASSICAL CONTROLLERS ON NONLINEAR VIBRATIONS ANALYSIS OF PIEZOELECTRIC NANORESONATOR

Sayyid H. Hashemi Kachapi[1], Sayyideh Gh. Hashemi Kachapi[2]

[1]Department of Mechanical Engineering, Faculty of Engineering and Technology,
University of Mazandaran, Babolsar, Iran
[2]Department of Physics, University of Kashan, Kashan, Iran

ORCID iDs: Sayyid H. Hashemi Kachapi   https://orcid.org/0000-0002-5384-9724
         Sayyideh Gh. Hashemi Kachapi   https://orcid.org/0009-0004-8518-4386

Abstract. *This study explores the influence of advanced continuum mechanics frameworks, specifically strain gradient theory (SGT), nonlocal theory (NLT), and Gurtin-Murdoch surface/interface theory (GMSIT), on the nonlinear vibrational characteristics of a piezoelectric nanoresonator (PENR). These findings are then juxtaposed with those derived from conventional continuum mechanics. The PENR is driven by a nonlinear electrostatic force, incorporating both static and dynamic voltage components, and is situated within a viscoelastic foundation of the Pasternak type. To dissect the nonlinear frequency response and stability of the PENR, a methodology combining Hamilton's principle, Galerkin's method, complex averaging techniques, and arc-length continuation is utilized. The analysis reveals that disregarding nanoscale and interfacial effects results in significant deviations from the actual vibrational response of the PENR. Notably, under diverse boundary constraints, the material length scale parameter (associated with SGT) induces a reduction in the PENR's rigidity, whereas the nonlocal scale parameter (associated with NLT) yields the opposite effect, enhancing stiffness. Moreover, the oscillation amplitude and the extent of instability predicted by the advanced theories (NLT and SGT) surpass those obtained via classical analysis. Fluctuations in the surface/interface parameters are demonstrated to exert a considerable influence on the PENR's normalized natural frequency, resonance frequency, resonance amplitude, nonlinear dynamics, and system stability, manifesting as either augmentations or diminutions contingent upon the specific parameter under consideration.*

Key words: *Piezoelectric nanoresonator, Nonlocal strain gradient theory, Gurtin–Murdoch surface/interface, Nonlinear frequency response, Complex averaging*

1. INTRODUCTION

The relentless march of technological innovation has spurred the proliferation of intelligent materials and adaptable structural systems [1, 2]. Within this domain, piezoelectric nanostructures, endowed with exceptional attributes, have garnered substantial interest, promising transformative applications across diverse sectors [3, 4]. Notably, piezoelectric shell architectures are extensively deployed in sensing and actuation technologies [5, 6]. Precise dynamic analysis and mathematical modeling of these nanoscale systems necessitate the incorporation of scale-dependent parameters. Consequently, advanced continuum theories, encompassing nonlocal [7], strain gradient [8], and Gurtin-Murdoch surface/interface [9] frameworks, are employed to probe their nonlinear vibrational and dynamic behaviors.

Drawing upon nonlocal elasticity principles, Feng et al. explored the axial vibrational characteristics of single-walled carbon nanotube-based mass sensors [10]. Soltani et al. [11] leveraged nonlocal elasticity to analyze the lateral-torsional buckling behavior of axially functionally graded nonlocal beams. Furthermore, Arefi demonstrated that an increase in the nonlocal parameter amplifies rotations, in-plane displacements, and transverse deflections within a piezoelectric nanoshell exhibiting double curvature [12]. Employing nonlocal strain gradient theory, Boyina et al. [13] investigated wave propagation in viscoelastic Timoshenko nanobeams under the influence of surface and magnetic field effects. Similarly, Liang et al. explored wave dispersion characteristics in lipid tubules, modeling them as shells, within the framework of nonlocal strain gradient theory [14]. Nonlinear vibration responses of piezoelectric nanosensors and nanoresonators have been addressed by Hashemi Kachapi et al. [15, 16] considering nonlocal and surface/interface effects.

Adopting the Gurtin-Murdoch approach to surface elasticity, Fang et al. [17, 18] investigated the nonlinear buckling, post-buckling, and vibration characteristics of piezoelectric nanostructures. Hashemi Kachapi et al. [19, 20] employed surface/interface and nonlocal strain gradient effects to investigate the effects of the small scale on the natural frequencies, nonlinear vibration, and stability analysis of piezoelectric nanostructures subjected to electrostatic and harmonic excitations.

It is noteworthy that, beyond the work of Hashemi Kachapi et al. [20], studies that consider simultaneously both surface and small-scale effects in piezoelectric materials remain scarce. Farrokhian et al. [21] investigated the vibration and damping behavior of smart sandwich nanotubes using nonlocal and surface piezoelasticity theories. Additionally, Ghorbani et al. [22] revealed that the material length scale (MLS) parameter augments natural frequency, while the nonlocal (NL) parameter diminishes it. Lovisi [23] explored the bending response of functionally graded cracked nanobeams, incorporating surface and nonlocal effects. Sun et al. [24] employed nonlocal and surface effects to analyze the buckling of piezoelectric nanoshells under external voltages and compressive loads. It is worth noting that in other works by Hashemi Kachapi et al. [25, 26], nonlinear vibration and stability analyses considering nonclassical effects were investigated for double-walled cases of piezoelectric nanostructures.

While prior research has extensively explored the vibrational and stability characteristics of piezoelectric nanostructures, a notable gap persists in studies that concurrently incorporate strain gradient, Gurtin-Murdoch surface/interface, and nonlocal effects. The present investigation extends the research trajectory initiated by Hashemi Kachapi et al [20]. However, it distinguishes itself through a distinct subject matter, particularly regarding the excitation forces and resulting findings, which are entirely independent of our previous

work. Unlike the earlier study, this analysis examines a nanostructure subjected to a complex nonlinear electrostatic excitation, encompassing both direct (DC) and alternating (AC) voltage components, while also considering the influence of a visco-Pasternak medium.

The primary objective of this study is to elucidate the impact of these combined effects on the nonlinear vibration and stability behavior of a piezoelectric nanoresonator, in comparison to predictions derived from classical continuum theory. To achieve this, a comprehensive analytical framework is employed, integrating Hamilton's principle, the Galerkin method, and a hybrid complex averaging technique coupled with arc-length continuation. This methodology facilitates a direct comparison of three nonclassical theories- strain gradient theory (SGT), nonlocal theory (NLT), and Gurtin-Murdoch surface/interface theory (GMSIT)- with classical continuum theory (CT). Consequently, the study investigates the influence of nanoscale and surface/interface effects, the elastic medium, electrostatic and piezoelectric voltages, and other relevant parameters on the dimensionless natural frequency (DNF), pull-in voltage, nonlinear frequency response, and stability of the piezoelectric nanoresonator.

2. MATHEMATICAL FORMULATION

Fig. 1 depicts the configuration of a cylindrical nanoshell-based piezoelectric nanoresonator subjected to a visco-Pasternak medium and nonlinear electrostatic excitation.
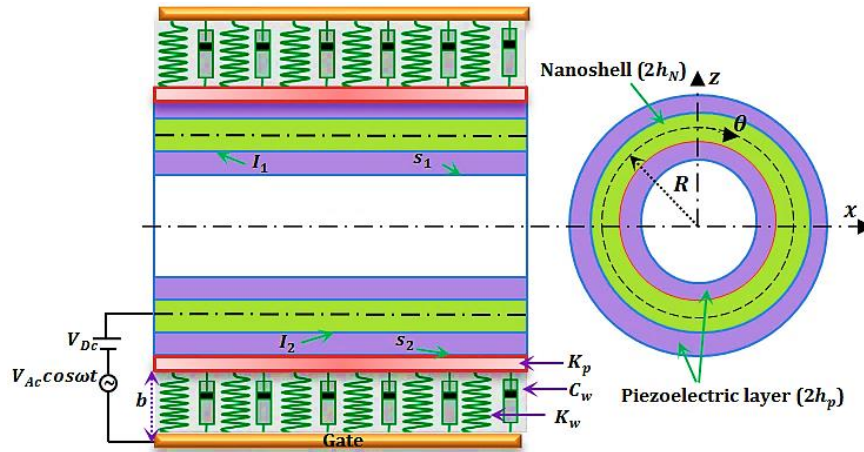

Fig. 1 A piezoelectric nanoresonator subjected to nonlinear electrostatic excitation

The nanoresonator is actuated by a superimposed electrostatic field, consisting of an alternating voltage component, V_{AC}, and a direct voltage component, V_{DC}. The geometric configuration of the piezoelectric nanoresonator is defined by the following parameters: mid-surface radius, R; axial length, L; piezoelectric material layer thickness, $2h_p$; and cylindrical shell thickness, $2h_N$. A Cartesian coordinate system is established with its origin positioned at the mid-surface of the nanoshell, where $x, \theta,$ and z denote the coordinates in the axial, circumferential, and radial directions, respectively. The supporting medium is characterized by a visco-Pasternak foundation, with K_w representing the Winkler foundation

stiffness coefficient, K_p denoting the shear layer stiffness of the Pasternak foundation, and C_w signifying the damping coefficient of the viscous medium for transverse motion. Additional physical and geometric properties of the nanostructure are detailed in Hashemi Kachapi et al. [19].

2.1. Governing Equations

This section delineates the derivation of the governing equations of motion and associated boundary conditions for the piezoelectric shell, utilizing Hamilton's principle:

$$\int_0^t \left(\delta T - \delta \pi + \delta w_{vf} + \delta w_e \right) dt = 0, \tag{1}$$

In this expression, δT, $\delta \pi$, δw_{vf} and δw_e represent the first variations of strain energy, kinetic energy, work done by the viscoelastic foundation, and work done by the nonlinear electrostatic excitation, respectively. It is crucial to note that all constitutive relations, coefficients, and expressions related to nonlocal strain gradient theory, surface/interface theory, nonlocal strain gradient surface/interface theory, nanoscale stress-strain relationships, and the physical and geometric properties employed herein are comprehensively detailed in Hashemi Kachapi et al [20]. The first variation of strain energy, $\delta \pi$, is expressed as:

$$\delta \pi = \int_0^L \int_0^{2\pi} \left\{ \begin{array}{l} N_{xx} \left(\frac{\partial \delta u}{\partial x} + \frac{\partial w}{\partial x} \frac{\partial \delta w}{\partial x} \right) - M_{xx} \left(\frac{\partial^2 \delta w}{\partial x^2} \right) + N_{\theta\theta} \left(\begin{array}{l} \frac{1}{R} \left(\frac{\partial \delta v}{\partial \theta} + \delta w \right) \\ + \frac{1}{R^2} \frac{\partial w}{\partial \theta} \frac{\partial \delta w}{\partial \theta} \end{array} \right) \\ -M_{\theta\theta} \left(\frac{1}{R^2} \frac{\partial^2 \delta w}{\partial \theta^2} \right) + N_{x\theta} \left(\begin{array}{l} \frac{1}{R} \frac{\partial \delta u}{\partial \theta} + \frac{\partial \delta v}{\partial x} \\ + \frac{1}{R} \frac{\partial \delta w}{\partial x} \frac{\partial w}{\partial \theta} \\ + \frac{1}{R} \frac{\partial w}{\partial x} \frac{\partial \delta w}{\partial \theta} \end{array} \right) - M_{x\theta} \left(\frac{2}{R} \frac{\partial^2 \delta w}{\partial x \partial \theta} \right) \end{array} \right\} R d\theta dx \tag{2}$$

The first variation of kinetic energy can then be expressed as: In Eq. (2), the force resultants, N, and moment resultants, M, are defined as specified in Hashemi Kachapi et al. [19]. The first variation of kinetic energy is given by:

$$\delta \int_{t_1}^{t_2} T dt = - \int_{t_1}^{t_2} \iint \left\{ I \left(\left(\frac{\partial^2 u}{\partial t^2} \right) \delta u + \left(\frac{\partial^2 v}{\partial t^2} \right) \delta v + \left(\frac{\partial^2 w}{\partial t^2} \right) \delta w \right) \right\} R d\theta dx dt \tag{3}$$

where

$$I = \int_{-h_N}^{h_N} \rho_N \, dz + \int_{-h_N-h_p}^{-h_N} \rho_p \, dz + \int_{h_N}^{h_N+h_p} \rho_p \, dz + \rho^{S,I} = 2 \left(\begin{array}{c} \rho_N h_N + \rho_p h_p \\ + \rho^S + \rho^I \end{array} \right) \tag{4}$$

The first variations of the work done by the viscoelastic foundation and the nonlinear electrostatic excitation, are expressed as [19, 20, 27]:

$$\delta W_{vf} = - \int_0^L \int_0^{2\pi} \int_0^w \left(K_w w - K_p \nabla^2 w + C_w \frac{\partial w}{\partial t} \right) \delta w \, R d\theta dx, \tag{5}$$

$$\delta W_e = \int_0^L \int_0^{2\pi} \int_0^w \frac{\pi \Upsilon (V_{DC} + V_{AC} \cos(\omega t))^2}{\left(\sqrt{(b-w)(2R+b-w)} \left[\cosh^{-1} \left(\frac{1+}{\frac{b-w}{R}} \right) \right]^2 \right)} \delta w \, R d\theta dx \tag{6}$$

The explicit definitions of all coefficients and expressions presented in Eqs. (5) and (6) are provided in Hashemi Kachapi et al. [19, 20].

Substituting Eqs. (2-6) into Eq. (1) results in the derivation of the governing equations of motion and associated boundary conditions for the piezoelectric nanoresonator (PENR), as comprehensively documented in Hashemi Kachapi et al. [19, 20]. By employing the dimensionless parameters defined in Hashemi Kachapi et al. [19], and subsequently incorporating nonlocal and material length scale effects, along with nonlocal strain gradient surface/interface effects (as detailed in Hashemi Kachapi et al [20]), the dimensionless governing equations are obtained.

$$(1 - \bar{\eta}\,\bar{\nabla}^2)\begin{pmatrix} \alpha_{1u}\frac{\partial^2\bar{u}}{\partial\xi^2} + \alpha_{2u}\frac{\partial^2\bar{u}}{\partial\theta^2} + \alpha_{3u}\frac{\partial^2\bar{v}}{\partial\xi\partial\theta} + \alpha_{4u}\frac{\partial\bar{w}}{\partial\xi} \\ +\alpha_{5u}\frac{\partial\bar{w}}{\partial\xi}\frac{\partial^2\bar{w}}{\partial\xi^2} + \alpha_{6u}\frac{\partial\bar{w}}{\partial\xi}\frac{\partial^2\bar{w}}{\partial\theta^2} + \alpha_{7u}\frac{\partial^2\bar{w}}{\partial\xi\partial\theta}\frac{\partial\bar{w}}{\partial\theta} \end{pmatrix} = (1 - \bar{\mu}\,\bar{\nabla}^2)\frac{\partial^2\bar{u}}{\partial\tau^2}, \quad (7)$$

$$(1 - \bar{\eta}\,\bar{\nabla}^2)\begin{pmatrix} \alpha_{1v}\frac{\partial^2\bar{u}}{\partial\xi\partial\theta} + \alpha_{2v}\frac{\partial^2\bar{v}}{\partial\xi^2} + \alpha_{3v}\frac{\partial^2\bar{v}}{\partial\theta^2} + \alpha_{4v}\frac{\partial\bar{w}}{\partial\xi}\frac{\partial^2\bar{w}}{\partial\xi\partial\theta} \\ +\alpha_{5v}\frac{\partial^2\bar{w}}{\partial\xi^2}\frac{\partial\bar{w}}{\partial\theta} + \alpha_{6v}\frac{\partial\bar{w}}{\partial\theta} + \alpha_{7v}\frac{\partial\bar{w}}{\partial\theta}\frac{\partial^2\bar{w}}{\partial\theta^2} \end{pmatrix} = (1 - \bar{\mu}\,\bar{\nabla}^2)\frac{\partial^2\bar{v}}{\partial\tau^2}, \quad (8)$$

$$(1 - \bar{\eta}\,\bar{\nabla}^2)\begin{pmatrix} \alpha_{1w}\frac{\partial\bar{u}}{\partial\xi} + \alpha_{2w}\frac{\partial\bar{u}}{\partial\xi}\frac{\partial^2\bar{w}}{\partial\xi^2} + \alpha_{3w}\frac{\partial\bar{u}}{\partial\xi}\frac{\partial^2\bar{w}}{\partial\theta^2} + \alpha_{4w}\frac{\partial^2\bar{u}}{\partial\xi^2}\frac{\partial\bar{w}}{\partial\xi} + \alpha_{5w}\frac{\partial^2\bar{u}}{\partial\xi\partial\theta}\frac{\partial\bar{w}}{\partial\theta} \\ +\alpha_{6w}\frac{\partial^2\bar{u}}{\partial\xi\partial\theta}\frac{\partial\bar{w}}{\partial\theta} + \alpha_{7w}\frac{\partial\bar{u}}{\partial\theta}\frac{\partial^2\bar{w}}{\partial\xi\partial\theta} + \alpha_{8w}\frac{\partial^2\bar{u}}{\partial\theta^2}\frac{\partial\bar{w}}{\partial\xi} + \alpha_{9w}\frac{\partial\bar{v}}{\partial\xi}\frac{\partial^2\bar{w}}{\partial\xi\partial\theta} \\ +\alpha_{10w}\frac{\partial^2\bar{v}}{\partial\xi^2}\frac{\partial\bar{w}}{\partial\theta} + \alpha_{11w}\frac{\partial^2\bar{v}}{\partial\xi\partial\theta}\frac{\partial\bar{w}}{\partial\xi} + \alpha_{12w}\frac{\partial\bar{v}}{\partial\theta} + \alpha_{13w}\frac{\partial\bar{v}}{\partial\theta}\frac{\partial^2\bar{w}}{\partial\xi^2} \\ +\alpha_{14w}\frac{\partial\bar{v}}{\partial\theta}\frac{\partial^2\bar{w}}{\partial\theta^2} + \alpha_{15w}\frac{\partial^2\bar{v}}{\partial\theta^2}\frac{\partial\bar{w}}{\partial\theta} + \alpha_{16w}\bar{w} + \alpha_{17w}\bar{w}\frac{\partial^2\bar{w}}{\partial\xi^2} + \alpha_{18w}\bar{w}\frac{\partial^2\bar{w}}{\partial\theta^2} \\ +\alpha_{19w}\frac{\partial^2\bar{w}}{\partial\xi^2} + \alpha_{20w}\frac{\partial\bar{w}}{\partial\xi}\frac{\partial^2\bar{w}}{\partial\xi\partial\theta}\frac{\partial\bar{w}}{\partial\theta} + \alpha_{21w}\frac{\partial^2\bar{w}}{\partial\xi^2}\left(\frac{\partial\bar{w}}{\partial\xi}\right)^2 + \alpha_{22w}\frac{\partial^2\bar{w}}{\partial\xi^2}\left(\frac{\partial\bar{w}}{\partial\theta}\right)^2 \\ +\alpha_{23w}\frac{\partial^4\bar{w}}{\partial\xi^4} + \alpha_{24w}\left(\frac{\partial\bar{w}}{\partial\xi}\right)^2 + \alpha_{25w}\frac{\partial^4\bar{w}}{\partial\xi^2\partial\theta^2} + \alpha_{26w}\left(\frac{\partial\bar{w}}{\partial\xi}\right)^2\frac{\partial^2\bar{w}}{\partial\theta^2} \\ +\alpha_{27w}\frac{\partial^2\bar{w}}{\partial\theta^2} + \alpha_{28w}\frac{\partial^4\bar{w}}{\partial\theta^4} + \alpha_{29w}\frac{\partial^2\bar{w}}{\partial\theta^2}\left(\frac{\partial\bar{w}}{\partial\theta}\right)^2 + \alpha_{30w}\left(\frac{\partial\bar{w}}{\partial\theta}\right)^2 \\ +\alpha_{31w}\frac{\partial^4\bar{w}}{\partial\xi^2\partial\tau^2} + \alpha_{32w}\frac{\partial^4\bar{w}}{\partial\theta^2\partial\tau^2} + \alpha_{33w} \end{pmatrix}$$

$$= (1 - \bar{\mu}\,\bar{\nabla}^2)\begin{pmatrix} \frac{\partial^2\bar{w}}{\partial\tau^2} + \bar{C}_w\frac{\partial\bar{w}}{\partial\tau} + \bar{K}_w\bar{w} - \bar{K}_p\bar{\nabla}^2\bar{w} - \\ \dfrac{\bar{F}_e(\bar{V}_{DC} + \bar{V}_{AC}\cos(\bar{\omega}\tau))^2}{\sqrt{(m_1\bar{b}-\bar{w})(2m_4\bar{R}+m_1\bar{b}-\bar{w})} \times \left[\cosh^{-1}\left(1+\dfrac{m_1\bar{b}-\bar{w}}{m_4\bar{R}}\right)\right]^2} \end{pmatrix}, \quad (9)$$

where $\bar{\nabla}^2 = \frac{\partial^2}{\partial\xi^2} + m_0^2\frac{\partial^2}{\partial\theta^2}$ and the coefficients of $\alpha_{iu}(i=1..7), \alpha_{jv}(j=1..7)$ and $\alpha_{kw}(k=1..33)$ are defined in Hashemi Kachapi et al [20]. the corresponding boundary conditions, expressed in dimensionless form, are given by:

$$\bar{u}=0: \left(\begin{array}{c}\alpha_{1u}^{bc}\frac{\partial\bar{u}}{\partial\xi}+\alpha_{2u}^{bc}\frac{\partial\bar{v}}{\partial\theta}+\alpha_{3u}^{bc}\bar{w}\\+\alpha_{4u}^{bc}\left(\frac{\partial\bar{w}}{\partial\xi}\right)^2+\alpha_{5u}^{bc}\left(\frac{\partial\bar{w}}{\partial\theta}\right)^2\\+\alpha_{6u}^{bc}\end{array}\right)\delta\bar{u}_\xi\Bigg|_0^1 + \left(\begin{array}{c}\alpha_{7u}^{bc}\frac{\partial\bar{u}}{\partial\theta}+\alpha_{8u}^{bc}\frac{\partial\bar{v}}{\partial\xi}\\+\alpha_{9u}^{bc}\frac{\partial\bar{w}}{\partial\xi}\frac{\partial\bar{w}}{\partial\theta}\end{array}\right)\delta\bar{u}_\theta\Bigg|_0^{2\pi}=0, \quad(10)$$

$$\delta\bar{v}=0: \left(\begin{array}{c}\alpha_{1v}^{bc}\frac{\partial\bar{u}}{\partial\theta}+\alpha_{2v}^{bc}\frac{\partial\bar{v}}{\partial\xi}\\+\alpha_{3v}^{bc}\frac{\partial\bar{w}}{\partial\xi}\frac{\partial\bar{w}}{\partial\theta}\end{array}\right)\delta\bar{v}_\xi\Bigg|_0^1 + \left(\begin{array}{c}\alpha_{4v}^{bc}\frac{\partial\bar{u}}{\partial\xi}+\alpha_{5v}^{bc}\frac{\partial\bar{v}}{\partial\theta}+\alpha_{6v}^{bc}\bar{w}\\+\alpha_{7v}^{bc}\left(\frac{\partial\bar{w}}{\partial\xi}\right)^2+\alpha_{8v}^{bc}\left(\frac{\partial\bar{w}}{\partial\theta}\right)^2\\+\alpha_{9v}^{bc}\end{array}\right)\delta\bar{v}_\theta\Bigg|_0^{2\pi}=0, \quad(11)$$

$$\delta\bar{w}=0: \left(\begin{array}{c}+\alpha_{1w}^{bc}\frac{\partial\bar{u}}{\partial\xi}\frac{\partial\bar{w}}{\partial\xi}+\alpha_{2w}^{bc}\frac{\partial\bar{u}}{\partial\theta}\frac{\partial\bar{w}}{\partial\theta}+\alpha_{3w}^{bc}\frac{\partial\bar{v}}{\partial\xi}\frac{\partial\bar{w}}{\partial\theta}+\alpha_{4w}^{bc}\frac{\partial\bar{v}}{\partial\theta}\frac{\partial\bar{w}}{\partial\xi}\\+\alpha_{5w}^{bc}\bar{w}\frac{\partial\bar{w}}{\partial\xi}+\alpha_{6w}^{bc}\frac{\partial\bar{w}}{\partial\xi}+\alpha_{7w}^{bc}\frac{\partial^3\bar{w}}{\partial\xi^3}+\alpha_{8w}^{bc}\frac{\partial^3\bar{w}}{\partial\xi\partial\theta^2}\\+\alpha_{9w}^{bc}\frac{\partial\bar{w}}{\partial\xi}\left(\frac{\partial\bar{w}}{\partial\xi}\right)^2+\alpha_{10w}^{bc}\frac{\partial\bar{w}}{\partial\xi}\left(\frac{\partial\bar{w}}{\partial\theta}\right)^2+\alpha_{11w}^{bc}\frac{\partial^3\bar{w}}{\partial\xi\partial\tau^2}\end{array}\right)\delta\bar{w}_\xi\Bigg|_0^1=0, \quad(12)$$

$$\frac{\partial\bar{w}}{\partial\xi}=0: \left(\begin{array}{c}\alpha_{23w}^{bc}\frac{\partial^2\bar{w}}{\partial\xi^2}+\alpha_{24w}^{bc}\frac{\partial^2\bar{w}}{\partial\theta^2}\\+\alpha_{25w}^{bc}+\alpha_{26w}^{bc}\frac{\partial^2\bar{w}}{\partial\xi^2}\\+\alpha_{27w}^{bc}\frac{\partial^2\bar{w}}{\partial\theta^2}+\alpha_{28w}^{bc}\frac{\partial^2\bar{w}}{\partial\tau^2}\end{array}\right)\delta\left(\frac{\partial\bar{w}_\xi}{\partial\xi}\right)\Bigg|_0^1 + \left(\alpha_{29w}^{bc}\frac{\partial^2\bar{w}}{\partial\xi\partial\theta}\right)\delta\left(\frac{\partial\bar{w}_\theta}{\partial\xi}\right)\Bigg|_0^{2\pi}=0, \quad(13)$$

$$\frac{\partial\bar{w}}{\partial\theta}=0: \left(\alpha_{30w}^{bc}\frac{\partial^2\bar{w}}{\partial\xi\partial\theta}\right)\delta\left(\frac{\partial\bar{w}_\xi}{\partial\theta}\right)\Bigg|_0^1 + \left(\begin{array}{c}\alpha_{31w}^{bc}\frac{\partial^2\bar{w}}{\partial\xi^2}+\alpha_{32w}^{bc}\frac{\partial^2\bar{w}}{\partial\theta^2}\\+\alpha_{33w}^{bc}+\alpha_{34w}^{bc}\frac{\partial^2\bar{w}}{\partial\xi^2}\\+\alpha_{35w}^{bc}\frac{\partial^2\bar{w}}{\partial\theta^2}+\alpha_{36w}^{bc}\frac{\partial^2\bar{w}}{\partial\tau^2}\end{array}\right)\delta\left(\frac{\partial\bar{w}_\theta}{\partial\theta}\right)\Bigg|_0^{2\pi}=0. \quad(14)$$

The coefficients of $\alpha_{lu}^{bc}(l=1..9)$, $\alpha_{mv}^{bc}(m=1..9)$ and $\alpha_{nw}^{bc}(n=1..36)$ are defined in Hashemi Kachapi et al [20].

Utilizing the lsqcurvefit function within the MATLAB Toolbox, a nonlinear least-squares curve-fitting technique, the electrostatic force in Eq. (6) is approximated as a polynomial. Consequently, the dimensionless work performed by the electrostatic force can be represented as:

$$\delta W_e=\int_0^L\int_0^{2\pi}\left\{\int_0^{\bar{w}}\left(\frac{\bar{F}_e(\bar{V}_{DC}+\bar{V}_{AC}\cos(\Omega\tau))^2\times}{(\bar{C}_1+\bar{C}_2\bar{w}+\bar{C}_3\bar{w}^2+\cdots+\bar{C}_n\bar{w}^{n-1})}\right)\delta\bar{w}\right\}\delta\theta\delta\xi \quad(15)$$

which $\bar{C}_1-\bar{C}_n$ are constant.

2.2. Solution Procedure

To transform the governing partial differential equations into a set of ordinary differential equations, the Galerkin method is employed. The displacement field is approximated using a series expansion of generalized coordinates and mode functions, as follows [28]:

$$\begin{bmatrix} u(x,\theta,t) \\ v(x,\theta,t) \\ w(x,\theta,t) \end{bmatrix} = \sum_{m=1}^{M_1} \sum_{j=1}^{N} \begin{bmatrix} \begin{bmatrix} u_{m,j,c}(\tau)\cos(j\theta) \\ +u_{m,j,s}(\tau)\sin(j\theta) \end{bmatrix} \chi_{mj}(\xi) \\ \begin{bmatrix} v_{m,j,c}(\tau)\sin(j\theta) \\ +v_{m,j,s}(\tau)\cos(j\theta) \end{bmatrix} \phi_{mj}(\xi) \\ \begin{bmatrix} w_{m,j,c}(\tau)\cos(j\theta) \\ +w_{m,j,s}(\tau)\sin(j\theta) \end{bmatrix} \beta_{mj}(\xi) \end{bmatrix} +$$

$$\sum_{m=1}^{M_2} \begin{bmatrix} u_{m,0}(\tau)\chi_{m0}(\xi) \\ v_{m,0}(\tau)\phi_{m0}(\xi) \\ w_{m,0}(\tau)\beta_{m0}(\xi) \end{bmatrix} = \sum_{(i,r,s)=1}^{M_2+M_1\times N} \begin{bmatrix} u_i(\tau)\chi_i(\xi)\vartheta_i(\theta) \\ v_r(\tau)\phi_r(\xi)\alpha_r(\theta) \\ w_s(\tau)\beta_s(\xi)\psi_s(\theta) \end{bmatrix} \tag{16}$$

In the Galerkin method, the trial functions, $\chi_i(\xi)$, $\phi_r(\xi)$ and $\beta_s(\xi)$, must satisfy all geometric and natural boundary conditions. Substituting Eq. (16) into Eqs. (7-14) and applying the Galerkin procedure yields the reduced-order equation of motion:

$$[(K)_u^u + (K_{bc})_u^u]\{\bar{u}\} + [(K)_u^v + (K_{bc})_u^v]\{\bar{v}\} + [(K)_u^w + (K_{bc})_u^w]\{\bar{w}\} + \\ [(NL)_u^w + (NL_{bc})_u^w]\{\bar{w}^2\} = [(M)_u^u]\{\ddot{\bar{u}}\} + \bar{F}_{up}^{bc}, \tag{17}$$

$$[(K)_v^u + (K_{bc})_v^u]\{\bar{u}\} + [(K)_v^v + (K_{bc})_v^v]\{\bar{v}\} + [(K)_v^w + (K_{bc})_v^w]\{\bar{w}\} + \\ [(NL)_v^w + (NL_{bc})_v^w]\{\bar{w}^2\} = [(M)_v^v]\{\ddot{\bar{v}}\} + \bar{F}_{vp}^{bc}, \tag{18}$$

$$[(K)_w^u]\{\bar{u}\} + [(K)_w^v]\{\bar{v}\} + \left[(K)_w^w + (K_{bc})_w^w - (K_{vp})_w^w - (K_{e2})_w^w\right]\{\bar{w}\} + \\ [(NL)_w^u + (NL_{bc})_w^u]\{\bar{w}\bar{u}\} + [(NL)_w^v + (NL_{bc})_w^v]\{\bar{w}\bar{v}\} + \\ [(NL)_{w2}^w + (NL_{bc})_{w2}^w - (NL_{2e})_{w2}^w]\{\bar{w}^2\} + \\ [(NL)_{w3}^w + (NL_{bc})_{w3}^w - (NL_{3e})_{w3}^w]\{\bar{w}^3\} = \\ ([(M)_w^w + (M_{bc})_w^w])\{\ddot{\bar{w}}\} + ([(C)_w^w] + [(C_{bc})_w^w])\{\dot{\bar{w}}\}) + \bar{F}_{wp} + \bar{F}_{wp}^{bc} - \bar{F}_{we} - \\ \bar{F}_e \left\{ \begin{matrix} ((\bar{V}_{AC}\cos\bar{\omega}\tau)^2 + 2\bar{V}_{AC}\bar{V}_{DC}\cos\bar{\omega}\tau) \times \\ (\bar{C}_4(NL_e)_{w3}^w + \bar{C}_3(NL_e)_{w2}^w + \bar{C}_2(K_e)_w^w + \bar{C}_1\bar{F}_1) \end{matrix} \right\} \tag{19}$$

where all coefficients and phrases of Eqs. (17-19) are defined by Hashemi Kachapi [20] and only coefficients of visco-pasternak medium , $(K_{vp})_w^w$, are presented in following Eq. (20) of current work:

$$(K_{vp})_w^w = \iint \begin{pmatrix} \bar{k}_w\left(\beta_r\beta_o\psi_s\psi_p - \bar{\mu}(\beta_r\beta_o''\psi_s\psi_p + m_0^2\beta_r\beta_o\psi_s\psi_p'')\right) \\ -\bar{k}_p(\beta_r\beta_0''\psi_s\psi_p + m_0^2\beta_r\beta_o\psi_s\psi_p'') \\ +\bar{k}_p\bar{\mu}\begin{pmatrix} \beta_r\beta_0''''\psi_s\psi_p + 2m_0^2\beta_r\beta_0''\psi_s\psi_p'' \\ +m_0^4\beta_r\beta_o\psi_s\psi_p'''' \end{pmatrix} \end{pmatrix} d\xi\, d\theta, \tag{20}$$

To solve the nonlinear equations of the system (Eqs. 17-19), the complex averaging method combined with arc-length continuation is employed [19, 20, 29].

3. RESULTS AND DISCUSSIONS

Validation studies for piezoelectric nanostructures are documented in Hashemi Kachapi et al. [19, 20]. This section examines the influence of diverse material and geometric parameters, both with and without the inclusion of nonlocal, strain gradient, and surface/interface effects, on the dimensionless natural frequency, stability characteristics, and frequency response. Analyses are performed for clamped-clamped (CC), simply supported-simply supported (SS), clamped-simply supported (CS), and clamped-free (CF) boundary conditions. The surface and bulk material properties of the aluminum (Al) nanoshell and PZT piezoelectric layer are tabulated in Tables 1 and 2, respectively [19, 20].

Table 1 Surface and bulk properties of Al

$E_N[GPa]$	v_N	$\rho_N[kg/m^3]$	$\lambda^I[N/m]$	$\mu^I[N/m]$	$\tau_0^I[N/m]$	$\rho^I[kg/m^2]$
70	0.33	2700	3.786	1.95	0.9108	5.46×10^{-7}

Table 2 Surface and bulk properties of PZT-4

$C_{11p}[GPa]$	$C_{22p}[GPa]$	$C_{12p}[GPa]$	$C_{21p}[GPa]$	$C_{66p}[GPa]$	$E_p[GPa]$
139	139	77.8	77.8	30.5	95
v_p	$\rho_p[kg\ m^{-3}]$	$\eta_{33p}[10^{-8}\ F/m]$	$\lambda^S[N/m]$	$\mu^S[N/m]$	$\tau_0^S[N/m]$
0.3	7500	8.91	4.488	2.774	0.6048
$e_{31p}[C/m^2]$	$e_{32p}[C/m^2]$	$e_{31p}^S[C/m]$	$e_{32p}^S[C/m]$	$\rho^S[kg/m^2]$	
−5.2	−5.2	$−3 \times 10^{-8}$	$−3 \times 10^{-8}$	5.61×10^{-6}	

The remaining physical and geometrical parameters of the PENR used in the following results are listed in Table 3 [19, 20, 22].

Table 3 The material and geometrical parameters

$R[m]$	L/R	h_N/R	h_p/R	b/R	$C_w[N.S/m]$
1×10^{-9}	10	0.01	0.005	0.1	1×10^{-3}
$K_w[N/m^3]$	$K_p[N/m]$	$V_p[V]$	V_0	$V_{DC}[V]$	$V_{AC}[V]$
9×10^{17}	2.07	1×10^{-5}	1	1.5	0.5
$\mu[m^2]$	$\eta[m^2]$				
$\left(1 \times 10^{-10}\right)^2$	$(1 \times 10^{-11})^2$				

3.1. Nonlinear Frequency Response and Stability Analysis

This section compares the predictions of three nonclassical continuum theories-nonlocal theory (NLT), strain gradient theory (SGT), and Gurtin-Murdoch surface/interface theory (GMSIT)- with those of classical continuum theory (CT). The analysis investigates the impact of various geometric and material parameters, incorporating and excluding strain gradient, nonlocal, and surface/interface effects, on the dimensionless natural frequency (DNF), stability, and nonlinear frequency response of the piezoelectric nanoresonator (PENR). Arc-length continuation is employed as the numerical solution method, utilizing the PENR specifications provided in Tables 1-3. Specifically, the NLT analysis considers the nonlocal parameter, $\bar{\mu}$; the SGT analysis considers the material length scale parameters, the

$\bar{\mu}$ and $\bar{\eta}$ parameters; and the GMSIT analysis incorporates surface/interface (S/I) effects. Recognizing the substantial influence of surface/interface densities on nanostructure vibration, two distinct surface density cases, as defined in Table 4, are presented.

Table 4 Two case of surface density

Case 1		Case 2	
$\rho^I[kg/m^2]$	$\rho^S[kg/m^2]$	$\rho^I[kg/m^2]$	$\rho^S[kg/m^2]$
5.46×10^{-7}	5.61×10^{-6}	5.46×10^{-8}	5.61×10^{-7}

Figs. 2 and 3 illustrate the dimensionless natural frequencies of the piezoelectric nanoresonator (PENR) as a function of the dimensionless nonlocal scale parameter $\bar{\mu}$ and the dimensionless material length scale parameter $\bar{\eta}$, respectively, both with and without surface/interface effects. As depicted in Fig. 2, surface/interface densities corresponding to case 1 result in a reduction of PENR stiffness, leading to a lower dimensionless natural frequency compared to the absence of surface/interface effects. Conversely, surface/interface densities associated with case 2 induce an increase in PENR stiffness, consequently yielding a higher dimensionless natural frequency.
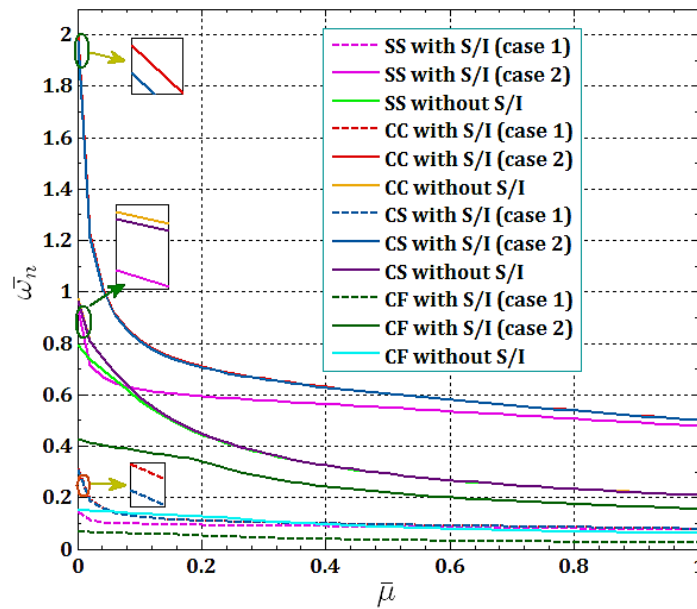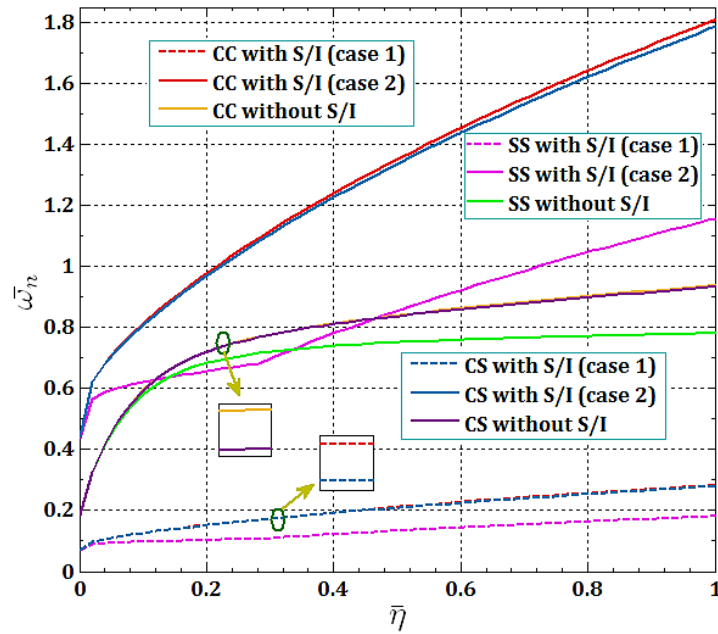

Fig. 2 Natural frequency vs. dimensionless nonlocal scale parameter $\bar{\mu}$ with $\bar{\eta} = 0.01$: influence of surface/interface effects for different boundary conditions

In all cases, the dimensionless natural frequency (DNF) decreases with increasing nonlocal scale parameter $\bar{\mu}$ with $\bar{\eta} = 0.01$, attributable to the reduced stiffness of the porous elastic nanorod (PENR). As shown in Fig. 3, the DNF increases with the dimensionless material length scale parameter $\bar{\eta}$ with $\bar{\mu} = 0.1$ across all scenarios, owing to the enhanced PENR stiffness. These results align with the previously discussed effects of surface/interface

densities. The trends in Figs. 2 and 3 demonstrate that the nonlocal scale parameter $\bar{\mu}$ and material length scale parameter $\bar{\eta}$ inversely influence PENR stiffness: $\bar{\mu}$ reduces stiffness, thereby lowering the DNF, while $\bar{\eta}$ enhances stiffness, increasing the DNF. Additionally, the dimensionless natural frequency associated with the CC boundary condition consistently exceeds those of CS, SS, and CF configurations. This disparity arises from the greater structural rigidity inherent to the CC boundary condition compared to others.

Fig. 3 Natural frequency vs. dimensionless material length scale parameter $\bar{\eta}$ with $\bar{\mu} = 0.1$: Influence of Surface/Interface Effects for Different Boundary Conditions

Fig. 4 illustrates the influence of the length to radius ratio ($\boldsymbol{L/R}$) on the dimensionless natural frequency (DNF) as a function of the dimensionless nonlocal scale parameter ($\boldsymbol{\bar{\mu}}$) for SS PENR. The results incorporate all surface/interface effects, with $\boldsymbol{\bar{\eta} = 0.01}$. As evident from Fig. 4, the dimensionless natural frequency (DNF) decreases with increasing values of both the length to radius ratio ($\boldsymbol{L/R}$) and the nonlocal scale parameter ($\boldsymbol{\bar{\mu}}$). This trend is attributed to the reduction in stiffness of the PENR.

Fig. 5 depicts the variation of the DNF as a function of the dimensionless material length scale parameter ($\boldsymbol{\bar{\eta}}$) for SS PENR under different $\boldsymbol{L/R}$ ratios. The analysis incorporates all surface/interface effects, with $\boldsymbol{\bar{\mu} = 0.1}$. As shown in the figure, the dimensionless natural frequency increases with the nonlocal parameter but decreases with the $\boldsymbol{L/R}$ ratio.
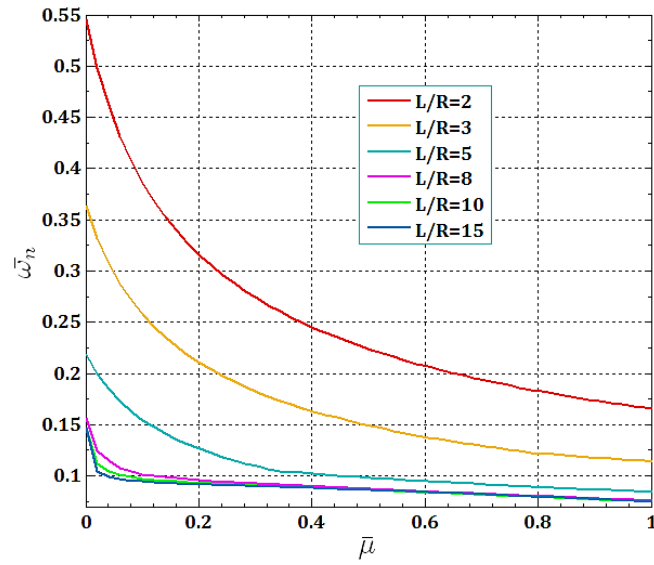
Fig. 4 Natural frequency vs. dimensionless nonlocal scale parameter $\bar{\mu}$:
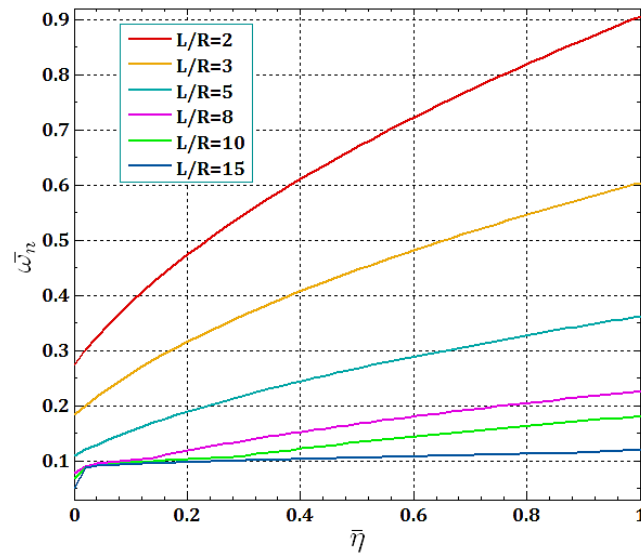influence of L/R ratio with all surface/interface effects and $\bar{\eta} = 0.01$

Fig. 5 Natural frequency vs. dimensionless material length scale parameter $\bar{\eta}$:
influence of L/R ratio with all surface/ interface effects and $\bar{\mu} = 0.1$

Fig. 6 compares the dimensionless natural frequency predicted by three nonclassical theories, NLT, SGT, and GMSIT, against the classical theory CT for SS PENR under varying piezoelectric thickness to radius ratios (h_p/R). As evident from the figure, the

GMSIT (Case 2) yields the highest DNF, indicating greater structural rigidity in this configuration compared to other cases. The lowest natural frequency is observed when GMSIT (case 1) is considered in combination with SGT, i.e. GMSIT+SGT ($\bar{\mu} = 0.1, \bar{\eta} = 0.01$), indicating that this combination results in the lowest system stiffness. Additionally, the natural frequency predicted by classical theory is higher than those predicted by NLT and SGT, demonstrating a reduction in system rigidity when these nonclassical theories are considered. Nonlocal theory predicts a higher natural frequency than strain gradient theory due to its greater rigidity. Surface/interface effects, depending on the surface/interface densities, can result in natural frequencies higher or lower than those predicted by classical theory. However, the combined application of NLT and SGT consistently yields a lower natural frequency than classical theory. Furthermore, the h_p/R ratio significantly influences the dimensionless natural frequency (DNF). An increase in this ratio leads to a decrease in PENR stiffness and, consequently, a decrease in the natural frequency.
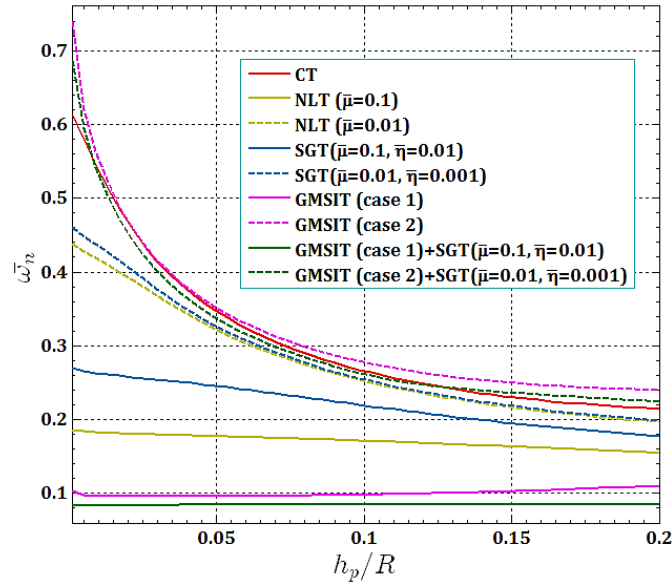
Fig. 6 Dimensionless natural frequency vs. piezoelectric thickness to radius ratio h_p/R: a comparison of non-classical and classical theories

Fig. 7 compares the dimensionless natural frequency predicted by three nonclassical theories, NLT, SGT, and GMSIT, with classical theory (CT) at various piezoelectric actuation voltages ($\bar{V}_p$) for SS PENR. It reiterates the effects of the various theories on natural frequencies, confirming the previous findings. The impact of piezoelectric voltage on the natural frequency varies across the different theories. GMSIT cases 1 and 2, as well as the combined GMSIT+SGT, exhibit the most significant changes, particularly at low surface density. In these instances, increasing voltage leads to increased system rigidity and, consequently, an initial rise in frequency, followed by a plateau with a slight slope. In contrast, other theories show minimal sensitivity of the PENR's natural frequency to piezoelectric voltage variations.
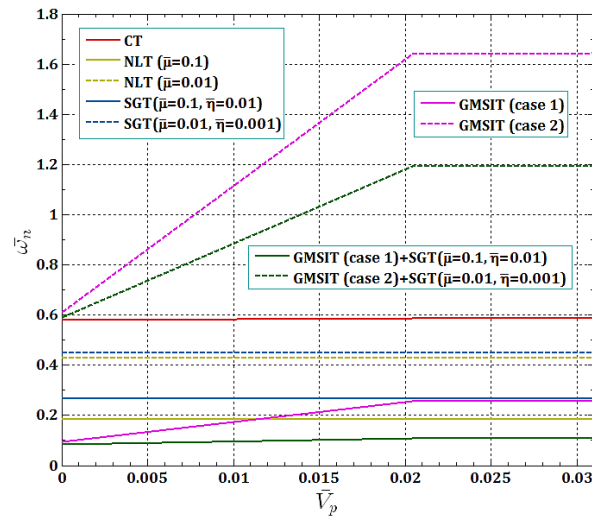
Fig. 7 Dimensionless natural frequency vs. piezoelectric voltage $\overline{V}_p$: comparison of nonclassical and classical theories

Fig. 8 presents a comparison of the dimensionless natural frequency predicted by NLT, SGT, GMSIT, and CT as a function of direct pull-in voltage (DC) for an SS nanoshell. The inclusion of surface/interface effects is known to enhance system rigidity, thereby necessitating a greater DC voltage to achieve pull-in. In contrast, the reduced stiffness associated with NLT, SGT, and CT leads to a lower pull-in voltage, with these theories predicting pull-in at roughly the same voltage level.
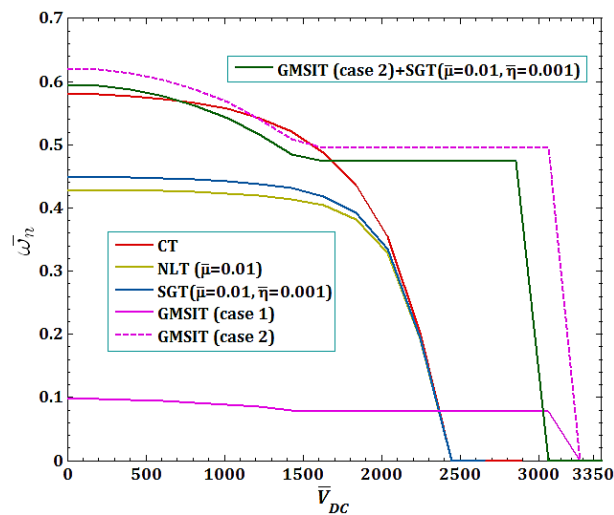
Fig. 8 Dimensionless natural frequency vs. direct pull-in voltage (DC) of SS PENR: a comparison of non-classical and classical theories

The nonlinear frequency response of SS and CC PENRs, as obtained from NLT, SGT, GMSIT, and CT, is compared in Figs. 9 and 10, respectively, for $\bar{V}_{DC} = 1.7$ and $\bar{V}_{AC} = 0.5$. As depicted in Fig. 9, the frequency analysis indicates that the incorporation of surface/interface effects in GMSIT case 2 (case 1) leads to a hardening (softening) of the SS PENR. This, in turn, results in an increase (decrease) in the resonant frequency and a corresponding decrease in the resonance amplitude.
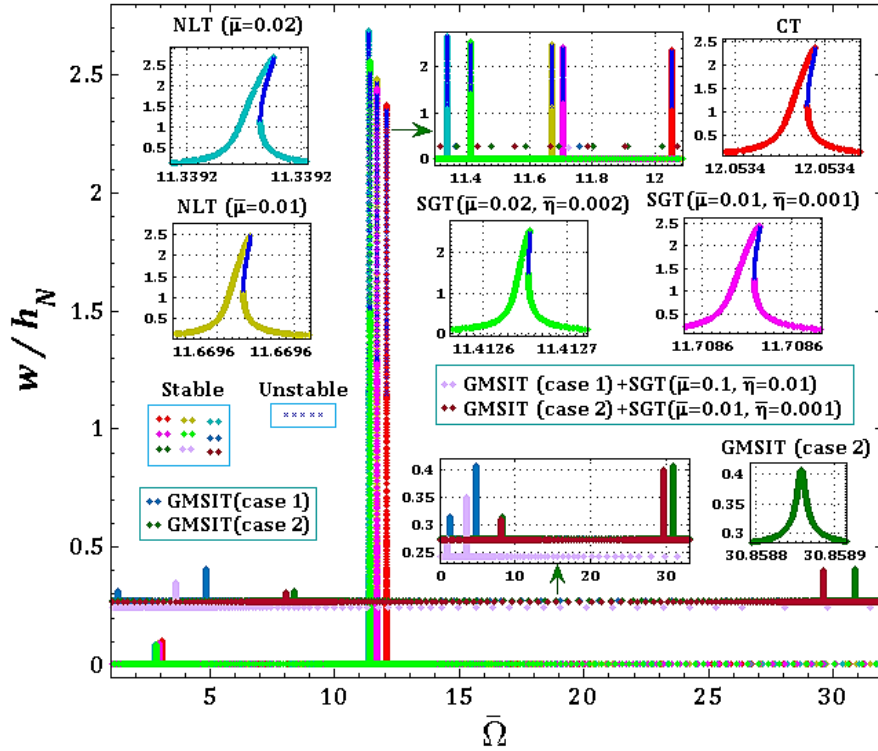

Fig. 9 Nonlinear vibration and stability analysis of SS PENR: comparison of non-classical and classical theories

The GMSIT model does not predict instability under the applied voltage conditions. Conversely, CT, NLT, and SGT exhibit instability, manifested as saddle-node bifurcations and nonlinear hardening behavior. The nonclassical theories, NLT and SGT, predict a larger oscillation amplitude and a wider instability range than the classical theory (CT). Moreover, an increase in $\bar{\tau}$ and $\bar{\eta}$ results in an amplified oscillation amplitude and an expanded instability range, accompanied by a reduction in resonance frequency.

As depicted in Fig. 10, an increase in the dimensionless nonlocal parameter results in a decrease in the resonance amplitude. This suggests that small-scale effects, as captured by the nonlocal model, enhance the flexibility of the CC PENR. Generally, the CC boundary condition yields result comparable to those of the SS boundary condition. However, a notable exception is observed in the SGT model, where an increase in $\bar{\tau}$ and $\bar{\eta}$ induces

nonlinear softening instability in the CC boundary condition, while the SS boundary condition exhibits nonlinear hardening instability.
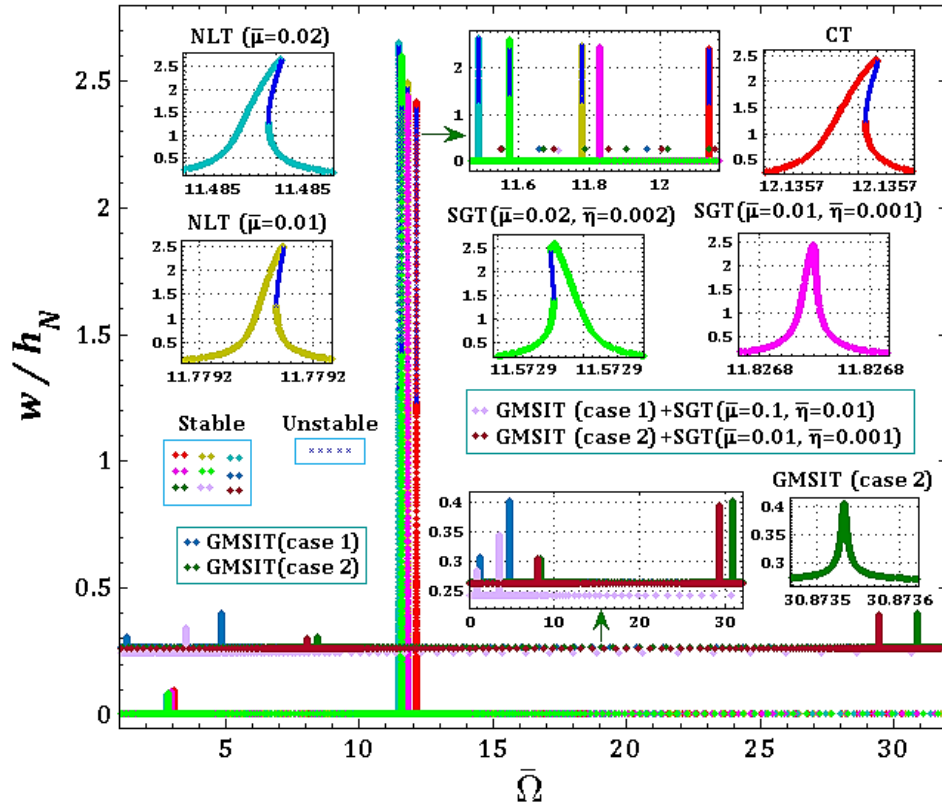

Fig. 10 Nonlinear vibration and stability analysis of CC PENR: comparison of nonclassical and classical theories

The frequency response and stability characteristics of the PENR, subjected to different direct ($\bar{V}_{DC}$) and alternating ($\bar{V}_{AC}$) voltages, are illustrated in Figs. 11-16. These figures compare the predictions of CT, NLT, SGT, GMSIT, and the combined theories GMSIT+NLT and GMSIT+SGT for SS boundary conditions.
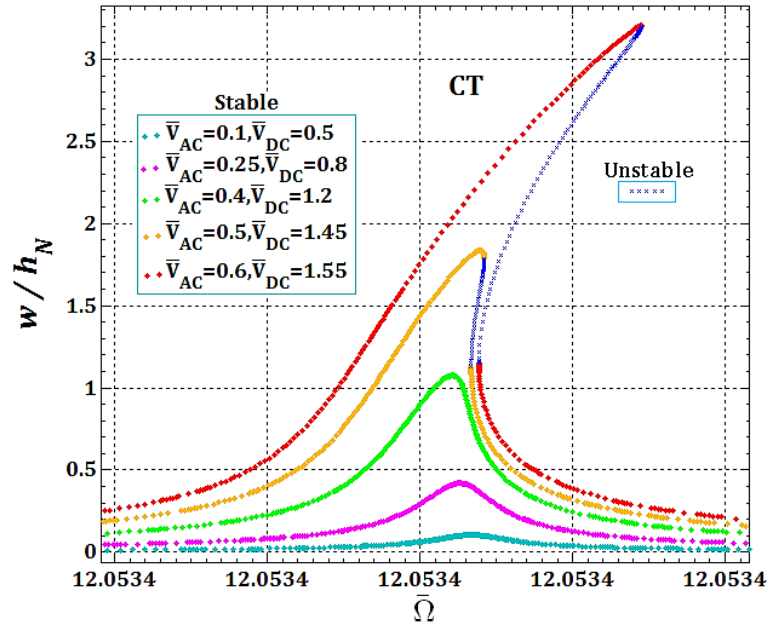
Fig. 11 Frequency response and stability analysis of SS PENR (CT) under varying DC and AC Voltages
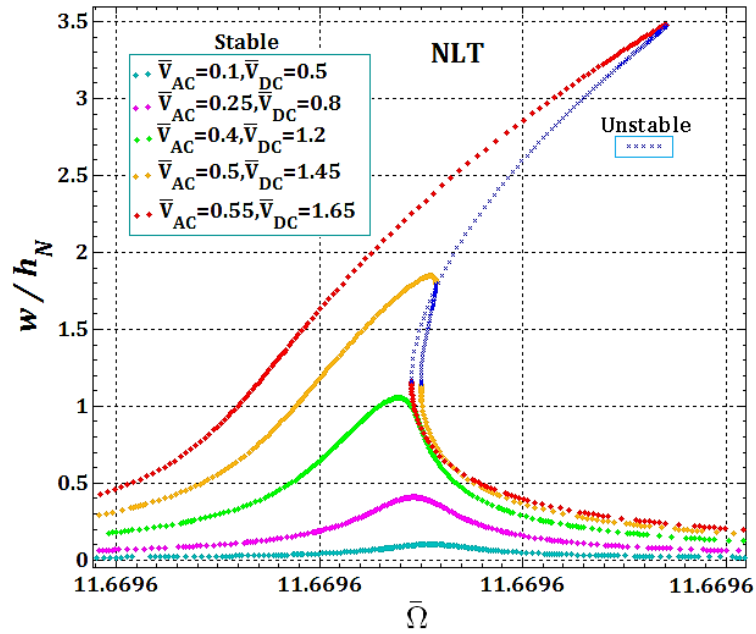

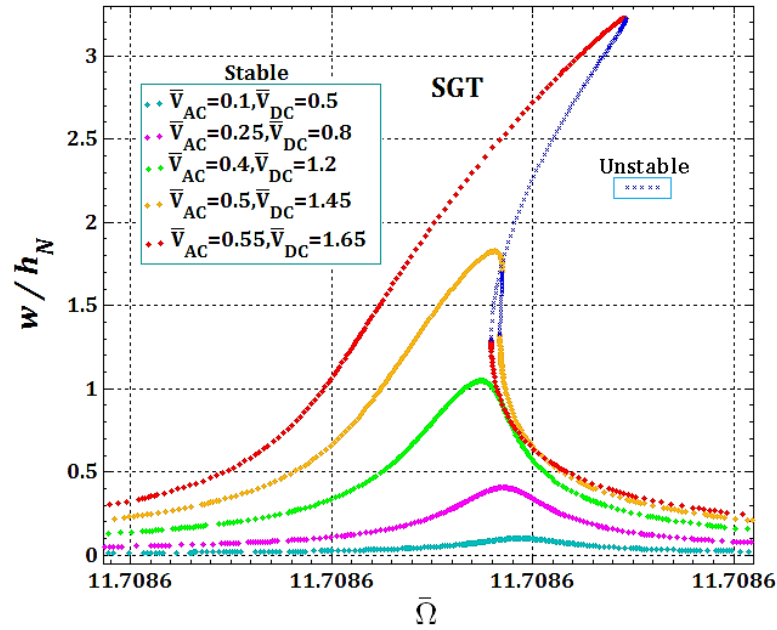**Fig. 12** Frequency response and stability analysis of SS PENR (NLT) under varying DC and AC Voltages

Fig. 13 Frequency response and stability analysis of SS PENR (SGT) under varying DC and AC Voltages
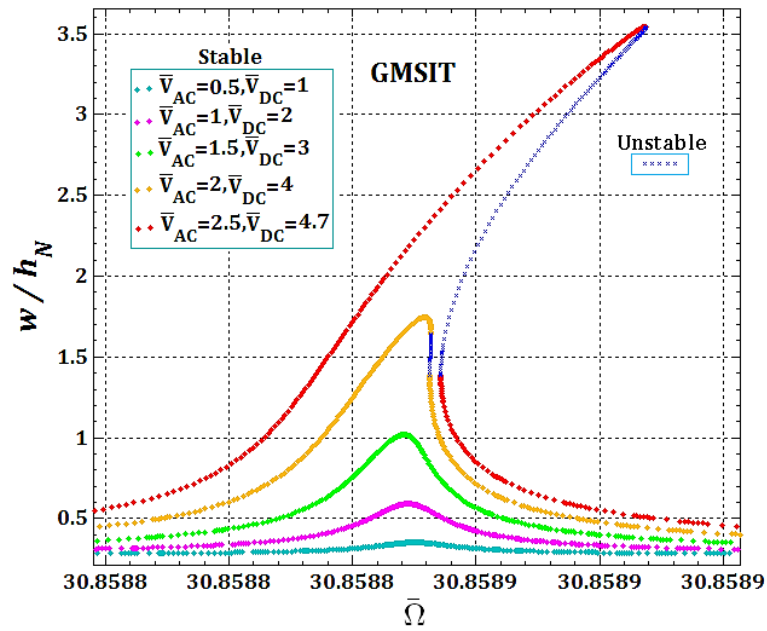

Fig. 14 Frequency response and stability analysis of SS PENR (GMSIT) under varying DC and AC Voltages
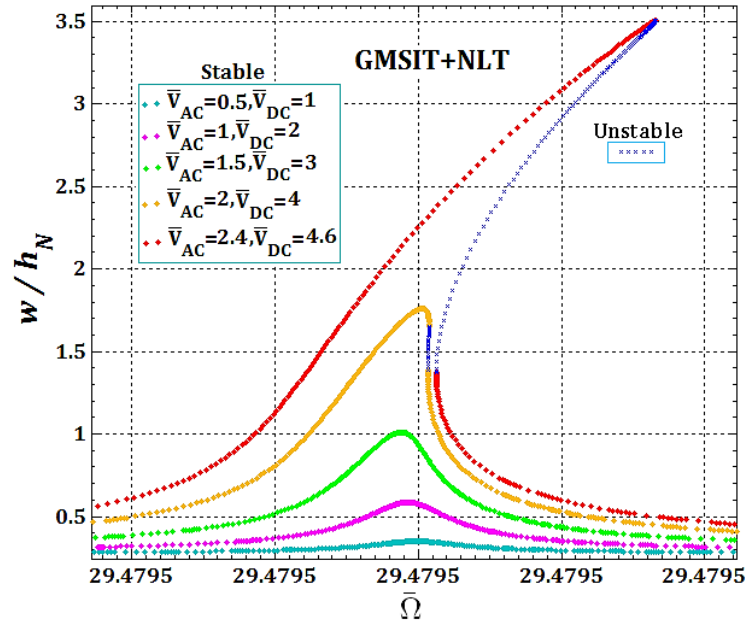
Fig. 15 Frequency response and stability analysis of SS PENR (GMSIT+NLT) under varying DC and AC Voltages
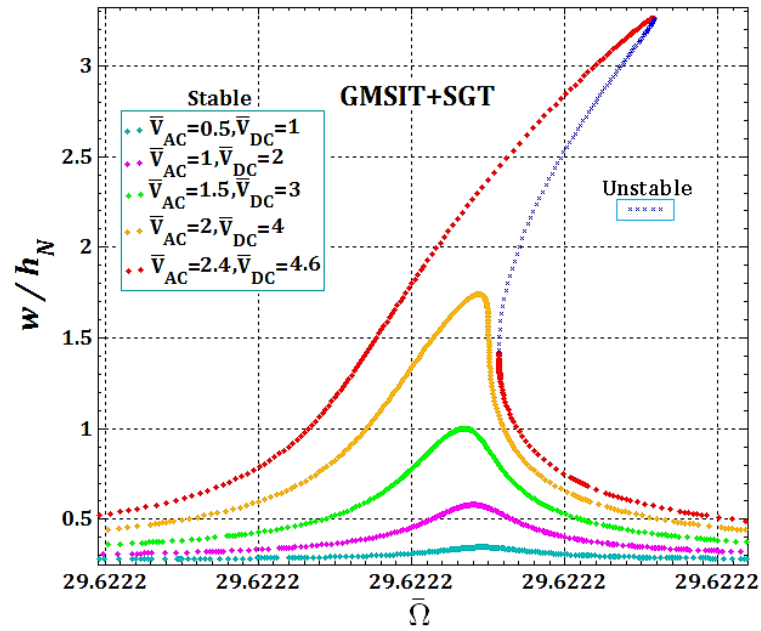

Fig. 16 Frequency response and stability analysis of SS PENR (GMSIT+SGT) under varying DC and AC Voltages

It can be concluded from Figs. 11-16 that the lowest resonance frequency for the unstable amplitude is related to Fig. 12 for the NLT theory (of course, in the absence of GMSIT case1, which has the lowest resonance frequency for the unstable amplitude) and the maximum value is related to Fig. 14 for the GMSIT (case2). As already mentioned, the three theories of CT, NLT, and SGT (respectively for Figs. 11-13), due to the softening of the system in these cases reach the unstable amplitude at lower voltages from DC and AC and in order to reach the unstable amplitude in the GMSIT theory, more voltages of DC and AC are needed. For example, according to the data in this work, CT, NLT and SGT theories in $\overline{V}_{AC} = 0.5$ and $\overline{V}_{DC} = 1.45$ reach unstable amplitude, while GMSIT theory and the simultaneous use of this theory with two non-classical theories, GMSIT + NLT (Fig. 15) and GMSIT + SGT (Fig. 16), are required to reach the unstable amplitude to $\overline{V}_{AC} = 2$ and $\overline{V}_{DC} = 4$ voltages. Furthermore, the results show that in all cases, with increasing of AC and DC voltages, the frequency amplitude is increased and the nanostructure shows nonlinear hardening behavior with saddle-node bifurcations.

Also, Figs. 17-22 present frequency response and stability analysis PENR for different values of direct ($\overline{V}_{DC}$) and alternating ($\overline{V}_{AC}$) voltages based on different theories of CT, NLT, SGT, GMSIT, GMSIT combined with NLT and SGT for CC boundary conditions. The results of Figs. 17-22 for CC PENR approximately are similar to Figs. 11-16 for SS PENR. It is clear from Figs. 11-22 that boundary condition SS than condition CC, in some approaches and under equal loading conditions, earlier reaches the instability region.
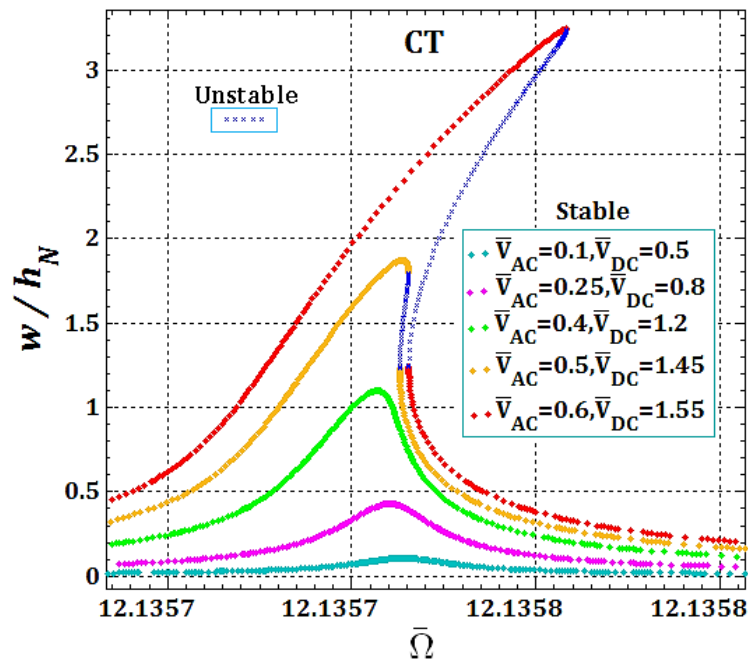

Fig. 17 Frequency response and stability analysis of CC PENR (CT) under varying DC and AC Voltages
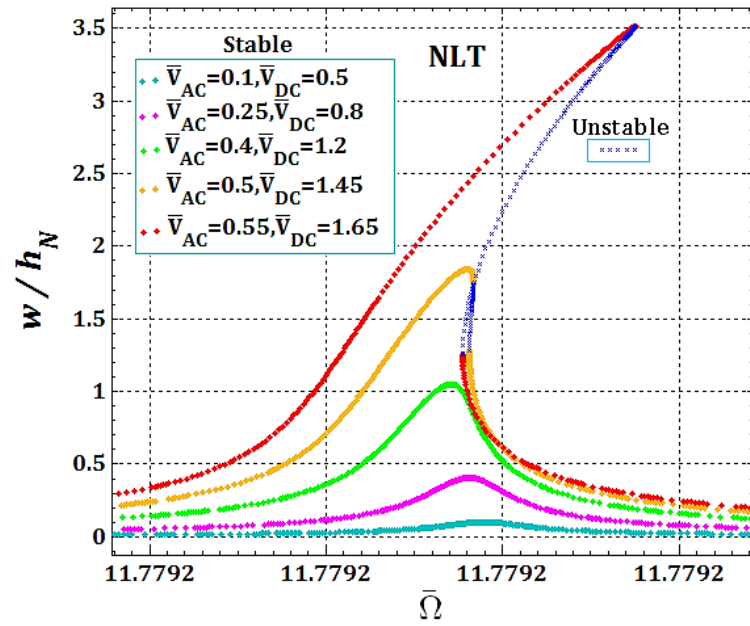
Fig. 18 Frequency response and stability analysis of CC PENR (NLT) under varying DC and AC Voltages
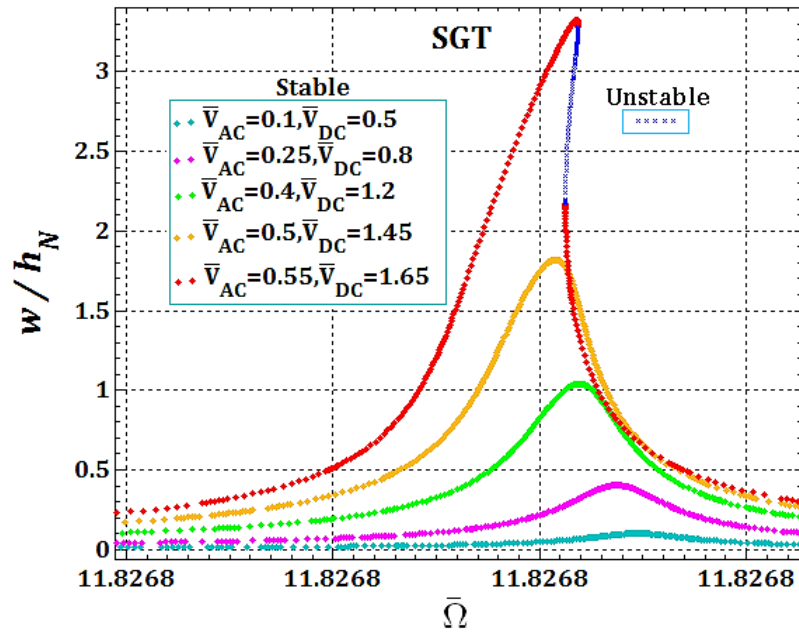

Fig. 19 Frequency response and stability analysis of CC PENR (SGT) under varying DC and AC Voltages
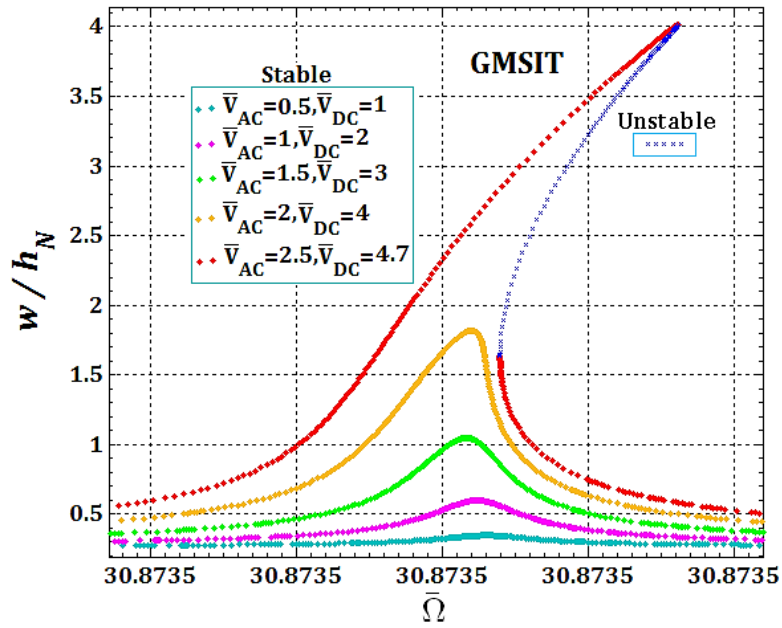
Fig. 20 Frequency response and stability analysis of CC PENR (GMSIT) under varying DC and AC Voltages
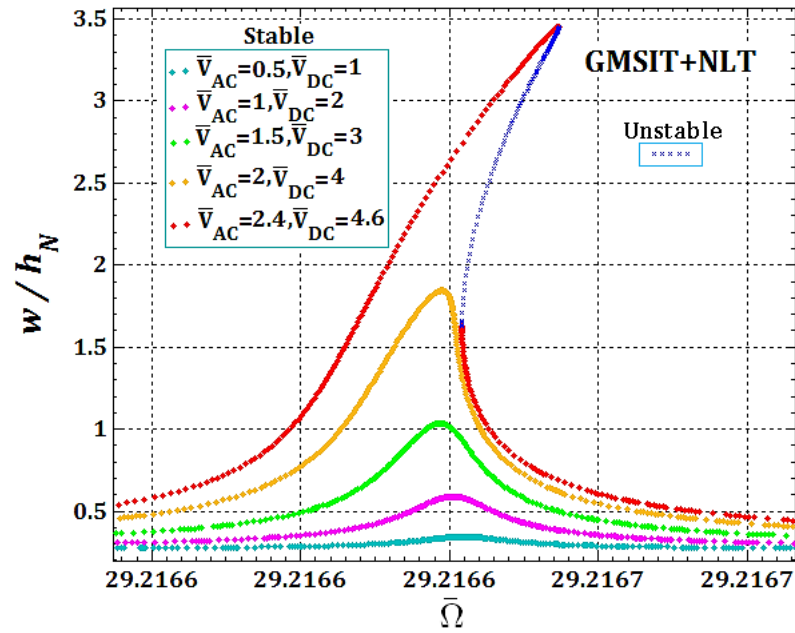

Fig. 21 Frequency response and stability analysis of CC PENR (GMSIT+NLT) under varying DC and AC Voltages
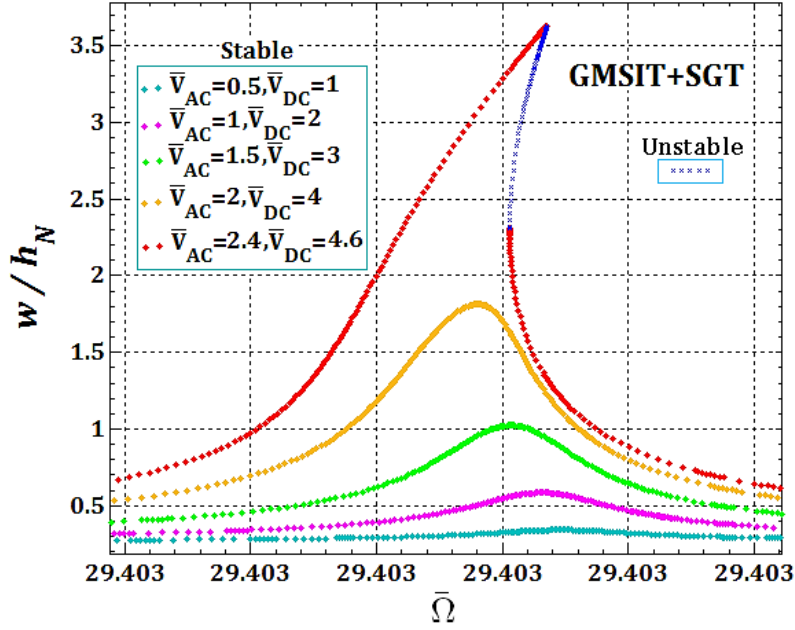
Fig. 22 Frequency response and stability analysis of CC PENR (GMSIT+ SGT) under varying DC and AC Voltages

4. CONCLUSION

This study investigates the influence of surface/interface parameters, specifically, Lamé's constants ($\lambda^{I,S}, \mu^{I,S}$), residual stress ($\tau_0^{I,S}$), piezoelectric constants ($e_{31p}^{Sk}, e_{32p}^{Sk}$), and mass density ($\rho^{I,S}$) on the pull-in instability, dimensionless natural frequency, and nonlinear dynamic response of a piezoelectric nanosensor. The nanosensor is subjected to two piezoelectric layers, a nonlinear electrostatic force, harmonic excitations, and structural damping. To achieve this, Hamilton's principle, assumed mode and Lagrange-Euler theories, along with arc-length continuation and complex averaging methods, are employed. The following conclusions are drawn from this investigation:

- Under conditions of lower surface/interface densities, an augmentation of stiffness is observed, resulting in an elevated natural frequency compared to scenarios lacking surface/interface effects. Conversely, higher surface/interface densities lead to a reduction in stiffness and a corresponding decrease in natural frequency.
- CF (CC) boundary condition with S/I case 1 has the lowest (highest) natural frequency: This indicates that when one end of the nanoresonator is clamped and the other is free, and the surface/interface properties correspond to case 1, the nanoresonator will vibrate at its slowest natural frequency.
- An increase in surface/interface Lamé's constants $\lambda^{I,S}$ and $\mu^{I,S}$, surface/interface residual stress $\tau_0^{I,S}$, and the magnitude of negative surface piezoelectricity constants e_{31p}^{Sk} and e_{32p}^{Sk}, results in an augmentation of the piezoelectric nanosensor (PENS)

stiffness. Consequently, this stiffness increase leads to a higher pull-in voltage in both the dimensionless natural frequency (DNF) and nonlinear dynamic response (NDR) analyses.

- An increase in surface/interface mass density $\rho^{I,S}$ leads to a reduction in the piezoelectric nanosensor (PENS) stiffness, resulting in a significant decrease in the dimensionless natural frequency (DNF). However, this increase in mass density does not significantly impact the pull-in voltage or the nonlinear dynamic response (NDR).

- In the dimensionless natural frequency (DNF) analysis, when surface/interface density $\rho^{I,S}$ and surface piezoelectric constants (e_{31p}^{Sk}, e_{32p}^{Sk}) are disregarded, the simply supported (SS) piezoelectric nanosensor (PENS) exhibits the maximum pull-in voltage across all surface/interface (S/I) configurations. However, in the nonlinear dynamic response (NDR) analysis of the SS PENS, the maximum pull-in voltage is observed in the absence of all surface/interface effects.

- In the nonlinear dynamic response (NDR) analysis, variations in surface/interface parameters lead to the system exhibiting either stable or unstable equilibrium points, with transitions occurring through saddle-node bifurcations.

REFERENCES

1. Marinković, D., Köppe, H., Gabbert, U., 2008, *Degenerated shell element for geometrically nonlinear analysis of thin-walled piezoelectric active structures*, Smart Materials and Structures, 17(1), 015030.
2. Nestorović, T., Marinković, D., Shabadi, S., Trajkov, M., 2014, *User defined finite element for modeling and analysis of active piezoelectric shell structures*, Meccanica, 49(8), pp. 1763-1774.
3. Chen, Q., Chatzigeorgiou, G., Meraghni. F., Javili. A., 2022, *Homogenization of size-dependent multiphysics behavior of nanostructured piezoelectric composites with energetic surfaces*, European Journal of Mechanics - A/Solids, 96, 104731.
4. Madunuri, C. S., Veena, E., Nagasamudram, S. K., Kadiyala, C. B. N., Mallikarjuna, A., Basha, B., 2022, *A Review on Piezoelectric Materials and Their Applications*, Crystal Research and Technology, 58(2), 2200130.
5. Milić, P., Marinković, D., Klinge, S., Ćojbašić, Ž., 2023, *Reissner-Mindlin Based Isogeometric Finite Element Formulation for Piezoelectric Active Laminated Shells*, Tehnicki Vjesnik, 30(2), pp. 416-425.
6. Rama, G., Marinković, D., Zehn, M., 2018, *Efficient three-node finite shell element for linear and geometrically nonlinear analyses of piezoelectric laminated structures*, Journal of Intelligent Material Systems and Structures, 29(3), pp. 345-357.
7. Eringen, A.C., 2002, *Nonlocal Continuum Field Theories*, Springer, New York, NY, USA.
8. Lim, C. W., Zhang, G., Reddy, J. N., 2015, *A higher-order nonlocal elasticity and strain gradient theory and its applications in wave propagation*, Journal of the Mechanics and Physics of Solids, 78, pp. 298-313.
9. Gurtin, M.E., Murdoch, A.I., 1978, *Surface stress in solids*, International Journal of Solids and Structures, 14(6), pp. 431-40.
10. Feng, J., Yu, H., Ma, S., Hao, S., Wu, R., 2022, *Axial vibration characteristics of carbon nanotube-based mass sensors containing nanoparticles using nonlocal elasticity theory*, Physica B: Condensed Matter, 634,413804 .
11. Soltani, M., Atoufi, F., Mohri, F., Dimitri, R., Tornabene, F., 2021, *Nonlocal elasticity theory for lateral stability analysis of tapered thin-walled nanobeams with axially varying materials*, Thin-Walled Structures, 159, 107268.
12. Arefi, M., 2018, *Analysis of a doubly curved piezoelectric nano shell: Nonlocal electro-elastic bending solution*, European Journal of Mechanics A/Solids, 70, pp. 226-237.
13. Boyina, K., Piska, R., 2023, *Wave propagation analysis in viscoelastic Timoshenko nanobeams under surface and magnetic field effects based on nonlocal strain gradient theory*, Applied Mathematics and Computation, 439, 127580.

14. Liang, C., Wang, Y.Q., Cao, D.Y., 2021, *Wave dispersion characteristics in lipid tubules considering shell model based on nonlocal strain gradient theory*, Results in Physics, 23, 103952.

15. Hashemi Kachapi, S.H., 2023, *Nonlinear vibration response of piezoelectric nanosensor: influences of surface/interface effects*, Facta Universitatis-Series Mechanical Engineering, 21(2), pp. 259-272.

16. Hashemi Kachapi, S.H., Hashemi Kachabi, S.G., 2025, *Nonclassical and Nonlinear Stability Analysis of Viscous Fluidic Piezoelectric Biomedical Nanosensor*, Spectrum of Mechanical Engineering and Operational Research, 2(1), pp. 59-77.

17. Fang, X.Q., Zhu, C.S., Liu, J.X., Liu, X.L., 2018, *Surface energy effect on free vibration of nano-sized piezoelectric double-shell structures*, Physica B, 529, pp. 41-56.

18. Fang, X.Q., Zhu, C.S., Liu, J.X., Zhao, J., 2018, *Surface energy effect on nonlinear buckling and postbuckling behavior of functionally graded piezoelectric cylindrical nanoshells under lateral pressure*, Materials Research Express, 5.4, 045017.

19. Hashemi Kachapi, S.H., Dardel, M., Mohamadi daniali, H., Fathi, A., 2019, *Pull-in instability and nonlinear vibration analysis of electrostatically piezoelectric nanoresonator with surface/interface effects*, Thin-Walled Structures, 143, 106210.

20. Hashemi Kachapi, S.H., Dardel, M., Mohamadi daniali, H., Fathi, A., 2019, *Nonlinear dynamics and stability analysis of piezo-visco medium nanoshell resonator with electrostatic and harmonic actuation*, Applied Mathematical Modelling, 75, pp. 279-309.

21. Farrokhian, A., Salmani-Tehrani, M., 2022, *Vibration and damping analysis of smart sandwich nanotubes using surface-visco- piezo-elasticity theory for various boundary conditions*, Engineering Analysis with Boundary Elements, 135, pp. 337-358.

22. Ghorbani, K., Mohammad, K., Rajabpour, i., Ghadiri, M., 2019, *Surface and size-dependent effects on the free vibration analysis of cylindrical shell based on Gurtin-Murdoch and nonlocal strain gradient theories*, Journal of Physics and Chemistry of Solids, 129, pp. 140-150.

23. Lovisi, G., 2023, Application of the surface stress-driven nonlocal theory of elasticity for the study of the bending response of FG cracked nanobeams, Composite Structures, 324, pp. 327-343.

24. Sun, J., Wang, Z., Zhou, Z., Xu, X.g, Lim, C.W., 2018, *Surface effects on the buckling behaviors of piezoelectric cylindrical nanoshells using nonlocal continuum model*, Applied Mathematical Modelling, 59, pp. 341-356.

25. Hashemi Kachapi, S.H., 2020, *Nonlinear and nonclassical vibration analysis of double walled piezoelectric nano-structure*, Advances in Nano Research , 9(4), pp. 277-294.

26. Hashemi Kachapi, S.H., Dardel, M., Mohamadi daniali, H., Fathi, A., 2020, *Nonlinear vibration and stability analysis of double-walled piezoelectric nanoresonator with nonlinear van der Waals and electrostatic excitation*, Journal of Vibration and Control, 9-10(26), pp. 680-700.

27. Farokhi, H., Païdoussis, M.P., Misra, A., 2016, *A new nonlinear model for analyzing the behaviour of carbon nanotube-based resonators*, Journal of Sound and Vibration, 378, pp. 56-75.

28. Amabili, M., 2008, *Nonlinear Vibrations and Stability of Shells and Plates*, Cambridge University Press, New York.

29. Manevitch, A.I., Manevitch, L.I., 2005, *The mechanics of Nonlinear Systems with Internal Resonance*, Imperial College Press, London.